European Journal of Cell Biology 103 (2024) 151383

Contents lists available at ScienceDirect

European Journal of Cell Biology

journal homepage: www.elsevier.com/locate/ejcb

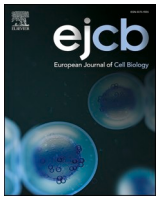

Helical motors and formins synergize to compact chiral filopodial bundles: A theoretical perspective

Ondrej Maxian [a,c,d], Alex Mogilner [a,b,*]

[a] Courant Institute, New York University, New York, NY 10012, USA
[b] Department of Biology, New York University, New York, NY 10012, USA
[c] Department of Molecular Genetics and Cell Biology, University of Chicago, Chicago, IL 60615, USA
[d] Institute for Biophysical Dynamics, University of Chicago, Chicago, IL 60615, USA

ARTICLE INFO

Keywords:
Actin bundle
Chirality
Filopodium
Filament buckling
Twisting
Formin

ABSTRACT

Chiral actin bundles have been shown to play an important role in cell dynamics, but our understanding of the molecular mechanisms which combine to generate chirality remains incomplete. To address this, we numerically simulate a crosslinked filopodial bundle under the actions of helical myosin motors and/or formins and examine the collective buckling and twisting of the actin bundle. We first show that a number of proposed mechanisms to buckle polymerizing actin bundles without motor activity fail under biologically-realistic parameters. We then demonstrate that a simplified model of myosin spinning action at the bundle base effectively "braids" the bundle, but cannot control compaction at the fiber tips. Finally, we show that formin-mediated polymerization and motor activity can act synergitically to compact filopodium bundles, as motor activity bends filaments into shapes that activate twist forces induced by formins. Stochastic fluctuations of actin polymerization rates and slower cross linking dynamics both increase buckling and decrease compaction. We discuss implications of our findings for mechanisms of cytoskeletal chirality.

1. Introduction

The cytoskeleton shapes cells, tissues and organs (Fletcher and Mullins, 2010). Actin filaments are crucial elements of the cytoskeleton, and are polar and chiral right-handed helices with distinct plus and minus ends (Jegou and Romet-Lemonne, 2020). Molecular polarity, helicity and chirality of actin filaments propagate to cytoskeletal arrays, cells, and tissues, which ultimately underlie important left-right asymmetries in development and complex organisms (Inaki et al., 2016). However, the mechanisms of this propagation remain largely unclear.

Two mechanical molecular processes were proposed to be the starting points for chirality generation in the cytoskeleton (Naganathan et al., 2016; Jegou and Romet-Lemonne, 2020). The first one is based on the action of formin, the "leaky capper" protein that stays on the growing plus end of the filament, thereby mediating the process of actin polymerization (Fig. 1A). Because of actin's helical structure, formin can rotate around the filament axis in the process of growth, or, if formin is fixed to a larger structure, an actin filament could rotate by being "extruded" from formin (Mizuno et al., 2011), in which case formin effectively applies a torque to the filament. The second symmetry-breaking process could be triggered by myosin molecular motors that in some cases move helically around actin filaments (Nishizaka et al., 1993), effectively applying both torque and force. Our goal here is to computationally examine how these two pathways of chirality emergence act in a small polar actin bundle.

There is no consensus yet on the chiral action of formins. On the one hand, Mizuno et al. observed actin filaments rotating clockwise (CW), if viewed from the plus end, when growing with a formin on the plus end (Mizuno et al., 2011). This would imply a formin-generated CW torque on the filament plus end. On the other hand, no supercoiling was observed when long actin filaments grew from formins attached to a substrate (Kovar and Pollard, 2004). If there is a formin-generated torque, then a sufficiently long filament must supercoil, so this result implies no or insignificantly weak torque. To explain this paradox, (Shemesh et al., 2005) proposed a mechanism where formins twist actin filaments until this twist is no longer energetically favorable, at which time a "screw" rotation dissipates the torsional strain. This model was expanded in the recent study (Li and Chen, 2022), which considered it in tandem with two other possible models of formin-actin interaction. The conclusion of that study is that, for some mechanisms, the formin can apply a rapidly fluctuating torque on the filament end, and that the net

* Correspondence to: Courant Institute, NYU, 251 Mercer St, New York, NY10012, USA.
E-mail address: mogilner@cims.nyu.edu (A. Mogilner).

https://doi.org/10.1016/j.ejcb.2023.151383
Received 24 July 2023; Received in revised form 19 December 2023; Accepted 30 December 2023
Available online 11 January 2024
0171-9335/© 2024 The Author(s). Published by Elsevier GmbH. This is an open access article under the CC BY license (http://creativecommons.org/licenses/by/4.0/).

Nomenclature

CW	(clockwise).
CCW	(counterclockwise).

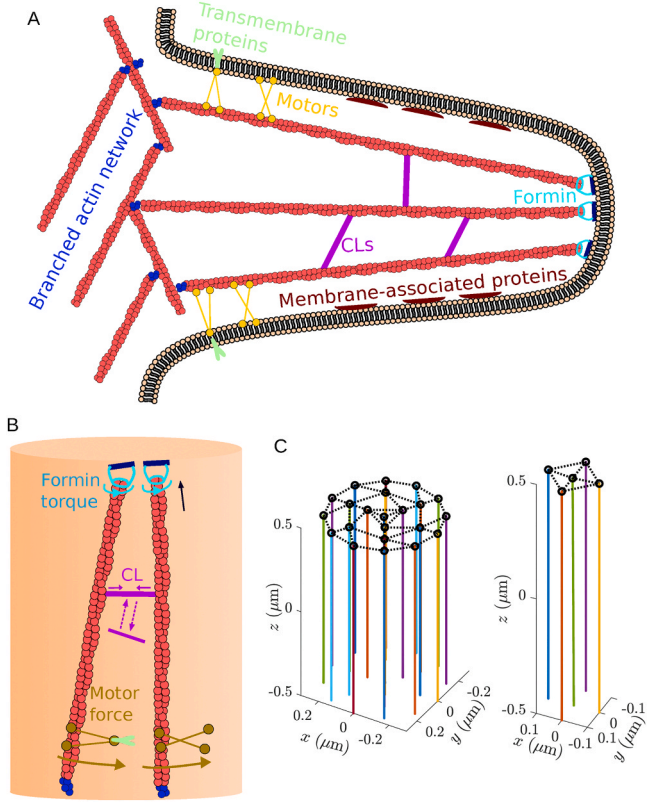

Fig. 1. Model filopodia. (A) Biological schematic. A filopodium is composed of long, almost parallel, cross-linked actin filaments emerging from a dense lamellipodial network at the base. In the model, the polymerization at the tip is driven by formins, which are attached to the membrane/protein tip complex. The filopodium is encased in a membrane, which is covered with a dense network of membrane-assocated and transmembrane proteins constituting an effective "sheath" around the actin bundle. Myosin motors associate with the sheath and interact with actin filaments. (B) Modeled mechanics of the bundle. We consider a system of fibers (slender inextensible rods), which are connected by crosslinks modeled as springs. The branched actin network at the base is reduced to a clamped condition, while the action of formin at the tips becomes a torque boundary condition (combined with polymerization at a variable rate). We model motors with their cargo domains attached to a firm cylindrical membrane/protein sheath and motor domains applying forces directed tangential to the cylindrical surface, with the main force component perpendicular to the bundle axis, and a minor force component downward along the axis. (C) Geometries of the two filopodial bundles that we use in this study. We consider a five-filament filopodium (right) and a 22-filament filopodium (left). The first is used to build intuition about the second, which has a realistic number of fibers. Initially, the fibers are connected at the tips by cross links.

torque would be on the order of 100 pN · nm (Li and Chen, 2022). Moreover, that model (Li and Chen, 2022) predicts that the torque can be both CW and counterclockwise (CCW).

Several reports pointed out that some myosin motors are helical, walking around actin filaments along a helical path, so when the motors are attached to a larger structure, they not only exert a force on a filament, but also apply torque to it. Tanaka et al. reported that muscle myosin could be either a CW or a CCW motor (Tanaka et al., 1992), while a later study proposed it to be exclusively CW motor (Nishizaka et al., 1993). (In the literature, the terms "right-" and "left-handed"' are often used for the helical motors; here, to avoid confusion, we call them CW and CCW (rotating the filament CW and CCW if viewed from plus end), respectively. Our view direction will always be from the plus end when mentioning CW or CCW rotation, and so we will skip mentioning the point of view henceforth.) Myosin V was reported to be a CCW spiral motor (Cheney et al., 1993; Ali et al., 2002a), while myosin X was shown to be a CCW helical motor that moves helically around actin bundles, rather than just single filaments (Sun et al., 2010). Myosin 1D was found to be a CCW motor (Lebreton et al., 2018). Twirling of actin by myosins II and V was observed in a gliding assay (Beausang et al., 2008).

These formin and myosin actions are relevant for actin bundle dynamics in filopodia, which are finger-like bundles which protrude from the cell edge and measure several to tens of microns in length and tenths of microns in diameter (Jacquemet et al., 2015). They consist of a parallel bundle of 10 to 30 actin filaments (Jacquemet et al., 2015) crosslinked by fascin (Aratyn et al., 2007) and other crosslinkers. The filaments polymerize and grow at the plus ends at the filopodial tip (Mallavarapu and Mitchison, 1999), while the bundle undergoes retrograde flow (away from the tip) driven by myosins at the filopodial base (Forscher and Smith, 1988; Aratyn et al., 2007). Filopodia play a variety of mechanical and sensory functions (Davenport et al., 1993) and are implicated in wound healing (Wood et al., 2002), cancerogenesis (Arjonen et al., 2011) and development (Fierro-González et al., 2013). Here, we consider slow-growing filopodia, in which electron microscopy shows actin filaments that are continuous all the way from the lamellipodium to the filopodial tip (Svitkina et al., 2003; Li et al., 2023).

Several examples of chiral filopodial behavior have been reported. For example, it was shown that actin filaments in filopodia flow toward the cell body, rotating in the CCW direction (Forscher and Smith, 1988). Individual filopodia were observed to rotate around their longitudinal axes in the CCW direction (Tamada et al., 2010), in a myosin-V-dependent way. Adherent filopodia, formed during the spreading of cells, tended to change the direction of their extension in a chiral fashion, acquiring a left-bent shape, if viewed from above, in a myosin X- and formin-dependent way (Li et al., 2023). Most notably, not only chiral movements, but also buckling and CCW helical rotation, as well as twisting and coiling of the filopodial actin bundle were reported (Leijnse et al., 2022). These deformations were myosin-, but not formin-dependent (Leijnse et al., 2022).

In filopodia, formins are at the tip, capping and elongating filaments' plus ends (Mellor, 2010; Alieva et al., 2019). Formins there are a part of the "tip complex," a dense large protein patch that may or may not be relatively rigid (Mellor, 2010). Some formin species attach to the membrane or cortex by a specialized domain, which in turn is elastically connected to the actin-elongating formin domains (Chesarone et al., 2010). Thus, there is a possibility that formins are mechanically restrained and apply a net torque to the growing filament ends. In our model, we will examine the possible CCW formin-generated net torque (Fig. 1A,B), and then also consider changes in model predictions when the torque is CW.

Various types of myosin motors are found at different parts of filopodia (Leijnse et al., 2022). For example, there is abundant expression of myosin V at the base of filopodia (Evans et al., 1997). There, myosin V can be connected to organelles or microtubules (Tamada et al., 2010). Myosin II is also located at the base of filopodia (Alieva et al., 2019), where it pulls on the bundled filaments (Sheetz et al., 1992; Medeiros et al., 2006; Nemethova et al., 2008). At filopodium initiation, myosin X molecules are recruited to the membrane near the base (Watanabe et al., 2010). Later, myosin X (Zhang et al., 2004), as well as integrins (Hu et al., 2014) become associated with the membrane and the sub-membranous protein coat surrounding the actin bundle (Fig. 1A). Leijnse et al. proposed that myosin X associates with integrins and that myosin V associates with cargo that is part of the sub-membranous

protein coat (Leijnse et al., 2015a), and that there are effective forces between the bundle filaments and integrin- and BAR-connected motors on the filopodial sheath. It is thus reasonable to assume that helical myosin motors there are associated with relatively rigid structures of the filopodial sheath, and that these motors' powerstrokes are applied to the outer filaments of the bundle, oriented diagonally relative to the filament centerlines, with components along the circumference of the filopodial bundle that rotate, or spin, the filaments around the filopodial axis. In the model, we will consider only CCW myosin-generated net torque (Fig. 1A,B), since we need only consider the direction of the myosin torque *relative* to that of formin (for which we consider both directions).

Filopodial actin bundles are wrapped with membrane, which affects the bundle mechanics (Pronk et al., 2008; Daniels and Turner, 2013). However, the inside of the filopodial membrane "sheath" is densely coated with a finely structured polymeric scaffold (Mattila and Lappalainen, 2008; Zhao et al., 2011; Linkner et al., 2014) that includes BAR domains, dynamin and cortactin copolymerized into ring-shaped complexes twined around the actin bundles (Yamada et al., 2013). These and other membrane-associated proteins can significantly modulate the shape and mechanics of the membrane (Mattila and Lappalainen, 2008).

The general questions we wish to answer in this study are: how do the chiral molecular mechanics of individual filament/myosin/formin actors play out on the scale of cytoskeletal arrays, creating collective chirality of actin filaments? Would not crosslinking interfere with collective chirality (one would imagine that stapling two filaments together prevents their rotation)? And, do myosins and formins cooperate or inhibit each other's actions? To address these questions, we numerically simulate a crosslinked filopodial bundle under chiral myosin and/or formin actions and quantitatively examine the collective buckling and coiling response. We find that the myosin spinning action effectively "braids" the actin bundle, compacting it, generating buckling, and enhancing the crosslinking. Stochastic fluctuations of actin polymerization rates also contribute to filament buckling and bending of the bundle. Faster turnover of transient crosslinks removes the constraints that give buckling, thereby attenuating it, but at the same time enhances coiling and compaction of the bundle. Formin-generated twisting is much less effective than myosin-generated spinning in inducing filopodial coiling; however, with myosin activity, co-rotating formins are essential to give proper bundle compaction.

2. Materials and methods: computational model

In a recent combined experimental-theoretical study, the emergence of chirality and twist in filopodia was modeled by considering the actin bundle as a continuum active polar gel (Leijnse et al., 2022). In our case, the relatively small number of filaments and associated molecules in filopodia makes a discrete approach, in which filaments are treated as elastic rods under the action of motor forces, more appropriate. Successful mathematical analyses of deformations of bent and twisted rods (Stump, 2000) and buckling of actin filaments (Berro et al., 2007) and bundles (Martiel et al., 2020) allow us to build a detailed mechanical model of a dynamic filopodial bundle. Here, for the sake of biologist readers, we explain the computational model, schematic of which is shown in Fig. 1A,B mostly in words; the details are described in the Supplemental Material (SM).

Actin filament mechanics: We adopt our published model (Maxian et al., 2022) to describe actin filaments as cylindrical, slender, inextensible elastic rods undergoing and resisting bending and twisting deformations. The filaments, which we sometimes call fibers, move, rotate and deform under the influence of the following forces and torques:

- Elastic bending force tends to straighten the filament's centerline.
- Elastic twisting force tends to minimize the filament's twist (relative rotation of neighboring cross sections around the centerline).
- Viscous resistance from the movement of the filament through the fluid it is immersed in.
- Elastic force between neighboring filaments generated by deformations of the crosslinks that couple pairs of filaments.
- Steric force between pairs of filaments that are in touch with each other, preventing one filament from passing through another.
- Active force generated by myosin motors, which we will call motor force for brevity.
- Active torques generated by formins.

Boundary conditions: The filaments at the base, $z = 0$, are cantilevered into the actin cortex of the cell and clamped, so their positions and orientations, as well as the orientations of the filament cross sections at the base, do not change in time. This formulation does not contradict the possibility of the retrograde flow of actin, because the growth of actin network at the lamellipodia leading edge effectively keeps the filopodial base at $z = 0$. The plus ends are free to move and twist.

Motor forces: As shown in Fig. 1A,B and discussed in the Introduction, we assume that helical motors are attached to the effectively rigid surface of the filopodial sub-membrane sheath and generate power strokes along a helical path on the cylindrical surface of a filament. The motors do not have to be immobilized to the sheath; if their cargo domains drift along the membrane with friction, this will also result in the effective helical force applied to the outer filaments of the bundle. The helical force has two components, one of which tries to move the filament retrogradely toward the filopodial base. We typically assume that this force component is significantly dampened because of the retrograde flow of the filopodial bundle (Evans et al., 1997). We discuss this in more detail in Section 3.3.2. The dominant force component is consequently directed along the circumference of the filopodium, so that this force spins the filaments around the long axis of the filopodium (in a circular trajectory). At a point $\boldsymbol{x}$, the force $\boldsymbol{f}^{(\mathrm{mot})}$ can be computed by first converting $\boldsymbol{x}$ into cylindrical coordinates (R, θ, z), and using these to define a vector tangent to the circle at $\boldsymbol{x}$, via $\boldsymbol{t} = (-\sin\theta, \cos\theta, 0)$. The force density is then given by $\boldsymbol{f}^{(\mathrm{mot})} = f_0^{(\mathrm{mot})}\boldsymbol{t}$ if $R \geq 3R_f/4$ and $z \leq c_m L$ (L is the filament length), so that the motors act only on the outer 1/4 and bottom c_m of the filopodium. Two parameters here defining the motor forces include $f_0^{(\mathrm{mot})}$, which is the magnitude of the force density in units of pN/μm, and c_m, the fraction of the filaments on which the motors act. As mentioned in the Introduction, we consider motors which spin filaments in a CCW direction around the filopodium.

Motor and formin torque: Depending on the location where motors apply force, the filament centerlines can experience torque. In most of our simulations, we will assume the motors apply force on the centerline, so that no torque is generated. Where noted, we will instead assume motor activity at the filament boundaries, which implies that motors exert a torque on the filament centerlines in the CCW direction (same direction as the motor forces) of magnitude $f_{\mathrm{mot}}^{(0)}a$, where a is the radius of the filaments. In Section 3.3.3, we compare simulations without motor torque to those that include it to determine its effect.

As discussed in the Introduction, it is sensible to model the action of formin via a fixed torque at the free end (where formin is bound). On the static ends, we use a no-rotation boundary condition, since we assume the filaments are clamped to the branched actin network there. In the absence of motor torque, the SM shows that the result of these boundary conditions is a constant angle of twist per unit length along the filament centerline. We reject as unphysical a boundary condition of a fixed angular velocity on the free end, and first consider a torque which tries to twist the filament in a CCW direction around the centerline, in the same direction as the motor spin. We also consider the effect of the opposite torque direction.

Crosslinking: In the model, the crosslinks connecting filament pairs are linear springs with finite rest length whose ends connect to the 1D centerlines of filaments by completely flexible joints. The crosslinking kinetics consist of unbinding with a constant, force-independent, rate,

and of possible crosslink binding to any pair of distinct filaments separated by a distance roughly equal to the crosslink rest length. When a crosslink unbinds, both of its ends dissociate from the filaments at once.

Steric forces: When any two points on distinct filaments become too close, we apply a strong, short-range repulsive force that prevents them from passing through each other, while not perturbing any dynamics of the non-overlapping filaments.

Modeling actin polymerization: Actin polymerization is modeled with elongation of a filament at its plus end with a certain rate $\dot{L}$. It was argued that in filopodia the polymerization is stochastic due to the relatively small size of the system and consequent large fluctuations of the actin monomer concentration (Lan and Papoian, 2008). One additional source of stochasticity could be persistently different chemical conditions of different filament plus ends, i.e. one filament's end associated with formin, another one with VASP protein, etc. To account for that, we first simulated growth rates constant in time but varying between the filaments. Then, we make the growth rate of each filament a random variable:

$$d\dot{L} = K_P(\dot{L}_0 - \dot{L})dt + \sigma\, dW, \tag{1}$$

where the constant $K_P = 2/\text{s}$ is chosen so that deterministic fluctuations relax to the base value $\dot{L}_0 = 0.5\ \mu\text{m/s}$ on timescales 0.5 s. The noise strength $\sigma = 0.05\sqrt{2K_P}$ is chosen so the (stationary) standard deviation of the growth rate is 0.05 μm/s. In simple words, the average rate is the same for all filaments, but each filament's rate independently fluctuates in time with certain variance. In the model, we neglect the experimentally-observed dependence of the polymerization rate on force and torque (Yu et al., 2017.

Model parameters: The elastic and mechanical parameters characterizing actin filaments, crosslinkers, motor and formin forces and torques, polymerization rates, crosslinker kinetics and viscous drag coefficients have all been measured or estimated in experimental literature. The full list of parameters, their values and respective citations are gathered in the Supplemental Table. We vary some of the parameters, such as formin torque, crosslinker kinetics and variance of the polymerization rates, to evaluate their effect on the bundle dynamics. The model predictions are relatively robust to few-fold changes in other parameters.

Quantification of the filopodial bundle's shape: In order to compare predicted filopodial dynamics and mechanics at different model regimes and parameters, we need to quantify the buckling and twisting of the filaments. Intuitively, we are interested in three parameters: the vertical extension of the filaments (in the direction of the bundle axis, or z direction), the filaments' bend, and their twist around the bundle axis. To quantify these, we transform the coordinates of each fiber from Cartesian to cylindrical, where the origin for the polar grid is set by the closest point on the central fiber. This gives a set of coordinates $(R(s), \theta(s), z(s))$ for each fiber. The vertical extension can then be tracked by looking at $z(L, t)$. The amount of twist can be quantified by the number of rotations around the axis of either the filament endpoints, $(\theta(L, t) - \theta(L, 0))/2\pi$, or their midpoints, $(\theta(L/2, t) - \theta(L/2, 0))/2\pi$. To study the amount of bend, we compute the curvature of the fibers (magnitude of the derivative of the tangent vector with respect to arclength) and average the curvature over the whole fiber (in the L^2 norm). We then normalize the curvature by the curvature of a circle of radius equal to the initial fiber length $L(0)$, which is $2\pi/L(0)$. Together, these statistics convey how bent and twisted the filaments are, and are similar to the quantifiers used in (Grason and Bruinsma, 2007; Tee et al., 2023) to measure chirality and twist. It is also useful to plot the traces or trajectories of the fiber endpoints over time projected onto the (x, y) plane.

Numerical procedure for simulating the actin bundle: At each computational step, current geometries of all fibers and engaged crosslinks are used to compute the elastic bending and twisting forces, steric and cross-linking forces, and motor and formin torques. By balancing the net forces and torques with viscous resistive forces, the linear and angular velocities of the filaments are calculated, and their geometries are updated. In addition, the increase of the filaments' lengths by polymerization is calculated, and some of the existing crosslinks are dissociated, while new crosslinks are engaged with filament pairs according to their dynamics. Marching in small time increments from step to step evolves the bundle. Here we use a time in seconds, which is a natural time scale for the cell-scale forces and viscosities. As discussed in the SM, twist equilibrates $\mathcal{O}(1/\epsilon^2)$ faster than bending (Powers, 2010), where ϵ is the fiber aspect ratio. As such, in our simulations twist deformations, while technically dynamic, are typically in a steady state controlled by the amount of the formin twist (see the SM).

3. Results

Our results section is laid out as follows: in Section 3.1, we consider simulations with formin-mediated polymerization and torque, but without motors, demonstrating that there is no collective buckling or coiling in this case. We introduce motors without polymerization in Section 3.2, demonstrating that filaments in motor-induced coils tend to splay out. We combine the two mechanisms in Section 3.3, where we demonstrate that the motor-induced bending of fibers combines with formin-induced twist to compact bundles.

3.1. Polymerizing bundles without motors are typically straight

We first consider simulations of five-filament bundles, in which there is a central filament and four parallel peripheral filaments, the minus ends of which are located on the vertices of a square (right panel of Fig. 1C), with polymerization and no motor activity. We consider two potential mechanisms by which filopodia could take on bent shapes: filament supercoiling (Bibeau et al., 2023) and unequal polymerization rates.

3.1.1. Actin supercoiling above a critical twist density

Linear stability analysis of the model equations (see the SM) states that the critical twist, above which an actin filament supercoils, corresponds to 2.4 360-degree turns of the plus end. We test this prediction numerically by applying 2 turns to the plus end and observing that the filament relaxes to a straight shape, and then applying 3 turns to the plus end and observing that the filament supercoils (Fig. S1).

Figure S1 shows the complete phase diagram of supercoiling behavior as a function of twist density and filament length, which comes from (S26) in the SM. The results of (Bibeau et al., 2023), who for small applied forces found a supercoiling threshold at roughly 0.2 rotations per micron with filaments of length 7–20 μm, validate our physical model. According to our estimates, the characteristic formin-generated torque $N_L = 0.1\ \text{pN} \cdot \mu\text{m}$ will result in ≈ 0.4 turns per μm, so formin will not generate supercoiling unless filaments become 6 μm long (red circle in Fig. S1), which we will not consider here.

3.1.2. Buckling generated by polymerization, alleviated by transient crosslinking

Another way to get a nontrivial shape of the filopodium is polymerization with unequal or varying rates. To illustrate this, we first consider an extreme case in which the central filament is the only one that grows in time. In Fig. S2, we simulate the five-filament bundle with the plus ends permanently crosslinked (imitating the filopodial tip complex), allowing the central filament to polymerize at rate 1 μm/s until it reaches length $L = 2$ μm. Initially, the central filament grows linearly, stretching the crosslinks. When the crosslinking force becomes too strong, the central filament buckles (at $t = 0.2$ s). The buckled filament then drags other filaments with it, which buckles the bundle as a whole.

Interestingly, supercoiling of filaments attenuates this effect. We illustrate this in Fig. S3, where we apply a larger amount of twist on the

central filament. The increased twist gives supercoiling of the *central* filament, which can then grow in length by increasing the length of coiling in the interior of the bundle, rather than buckling and pushing the peripheral filaments.

In Fig. 2, we extend the unequal polymerization concept to the more biologically-realistic scenario of filaments with varying polymerization rates centered around a constant mean. First, we consider the five-filament bundle with permanent crosslinks at the filament plus ends. Each filament has a prescribed random growth rate which is drawn at $t = 0$ from a normal distribution with mean 0.5 μm/s and varying standard deviation (0.2, 0.1, or 0.05 μm/s), and then does not change in time. To prevent fibers from getting too long, we stop fibers from lengthening when the length gets longer than double the initial length of 1 μm. One simulation with growth rate standard deviation 0.1 μm/s is shown in Fig. 2A.

In Fig. 2B, we show the average statistics for filopodia growth with the three different standard deviations in the growth rate. The statistics confirm the hunch that variance in the growth rates aids curvature. In Fig. 2B, we also consider the differences in the trajectories when we simulate without any formin torque (ligher colors), versus when the formin exerts a torque at the plus ends. We find that having a nonzero torque leads to fibers with higher average curvature. However, the effect is very slight, which indicates that torque on the fiber endpoint makes little difference when the fibers are fairly straight. Indeed, for straight fibers the translational force induced by twist is zero (see (S2)), so it makes sense that we see little impact on the dynamics in this case.

3.1.3. Dynamic crosslinking alleviates buckling

To understand how the bending behavior depends on the crosslinking turnover rate, we fix $k_{on}/k_{off} = 0.02$, but vary the values of the rates, so that the average number of bound links stays roughly constant (at 8–10 links) while the residence time of the links changes. In Fig. 2C, we show the same simulation of the buckling bundle as in Fig. 2A, but this time with *transient* CLs with off rate $k_{off} = 2.5$/s. We note how dynamic crosslinking alleviates the bending of the peripheral fibers – while the red filament still grows faster than the others, the transient nature of the links prevents it from taking the peripheral filaments with it.

To quantify this effect, we repeat the test of the previous section (with a mean growth rate of 0.5 μm/s and standard deviation of $\sigma = 0.2$ μm/s), but with transient links. Fig. 2D shows that links with longer residence times induce more bending of the filaments. However, even at the longest residence time of 0.4 s ($k_{off} = 2.5$/s), we still observe curvature which is 2 to 3 times smaller than the value for permanent crosslinkers located at the filopodium tip (green lines in Fig. 2B). Thus, transient crosslinkers allow for more variable growth rates without strong bending of the central shaft.

3.2. Motors can effectively braid filaments, aided by transient crosslinking

Whereas Section 3.1 focused on polymerization without motors, in this section we use the five-filament bundle to build intuition about the opposite process: motors without polymerization.

3.2.1. Motors with longer range give efficient braiding and compaction

We now add to the five-filament bundle an external force density that describes the action of helical motors that act near the filopodial boundary (the motors cannot reach the central filament). We begin with the simplest scenario, filaments *without* crosslinkers. In this case, Fig. 3A shows how the action of the motors rapidly twists the fibers into a braid with multiple turns. After the plus end makes about two turns relative to the base, the braiding motion is arrested because fiber elasticity and steric forces balance the motor turning action. The fundamental dynamics of the process are unchanged when we add transient crosslinking, since the motors always tend to drive the filaments into the braid.

How is it possible that the fibers are fully braided (and tightly wound) at the top, when the motors can only reach the outer quarter of the bundle? The explanation (Fig. 3A) is that fibers that reach the motor zone on the outside of the bundle are always getting pushed into the braid by the combination of motor activity (which twists them radially) and inextensibility (which prevents the fibers from stretching), and steric repulsion. Thus, once a fiber gets sufficiently wound, this combination of forces draws it into the braid, even as it loses access to the motors. Note especially the effect of this in the third frame of Fig. 3A, where we see filaments which tend to turn outward initially and are then redirected inward by the motors.

Let us now suppose that the motors can only reach the bottom half of the fibers, i.e., $c_m = 1/2$. In this case (Fig. 3B), the fibers at the bottom again start to form a braid, but, when the top half of the fiber relaxes outward, there is no motor activity to continue the braiding process and the bundle becomes stuck. The final state is a semi-braided state where the fiber endpoints sit roughly 0.2 μm away from the central filament (see endpoint projection in the right of Fig. 3B), which is twice as far as their initial position. Thus motors, while good for twisting and braiding, by themselves typically cannot keep the fiber bundles *compact*.

3.2.2. Transient crosslinking aids compaction

Seeing as the filaments in the top half of the bundle in Fig. 3B appear to be escaping from each other, it makes sense that crosslinking should help keep them together. This is indeed what we see in Fig. 3C, where we introduce transient cross linking (with $k_{off} = 5$/s and $k_{on} = 0.1$/s) into the simulation with motors covering half the length. The endpoint trajectories at the right of Fig. 3C show that the fiber endpoints no longer linearly escape the bundle, so that in the end only one (the red) of the peripheral fibers falls outside of the original boundary. Nevertheless, this process is dependent on having crosslinkers which can turn over fast enough to find and bind pairs of filaments which are on the verge of escape, and is imperfect because eventually the crosslinkers will unbind, and fibers will escape. Thus more transient crosslinking aids compaction, but is not sufficient to keep the bundle compact. While permanent crosslinking at the filament tips is an obvious solution to this problem, Section 3.1.2 hints that having more permanent crosslinkers might lead to more buckling, which decreases compaction. We study this more systematically in Section 3.4, where we give statistics that show an optimum for intermediate crosslink binding times.

3.3. Formins and motors synergize to twist and compress large filopodia

So far, we have discovered that polymerization gives relatively compact bundles of straight filaments, while motor activity gives bent bundles which tend to splay outwards in time. To demonstrate that there is a synergy between motor-driven bending and formin-generated twist, we turn to a larger bundle with 22 fibers (characteristic for filopodia) arranged into four rings (1, 3, 6, and 12 filaments). The rings are spaced 100 nm (the crosslinker rest length) apart, and fibers are positioned with uniform spacing around each ring (Fig. 1C). Starting with this initial geometry, we perform simulations with both motor activity and polymerization. The growth rate of each filament is a random variable which varies in time according to Eq. (1), tuned so that the standard deviation is 0.05 μm/s and the average growth rate of each filament is 0.5 μm/s. We also always distribute the motors in the bottom half of the filopodium, and use dynamic cross linkers with on rate $k_{on} = 0.2$/s and off rate $k_{off} = 10$/s.

What we are interested in is how the motor activity and the torque $N_L = 0.1$ pN $\cdot$ μm that the formin exerts on the fiber tips affect the overall chirality of the bundle. Thus, we will consider three sets of simulations: one with twisting and no motor activity (Fig. 4B), one with motor activity and no twisting (Fig. 4C), and one with both twisting and motor activity (Fig. 4A). These plots show three time points ($t = 0.2$, 0.8, and 2 s); for more time points see the supplementary movies, which show both side views and top views, as well as one movie of all three filopodia growing at once.

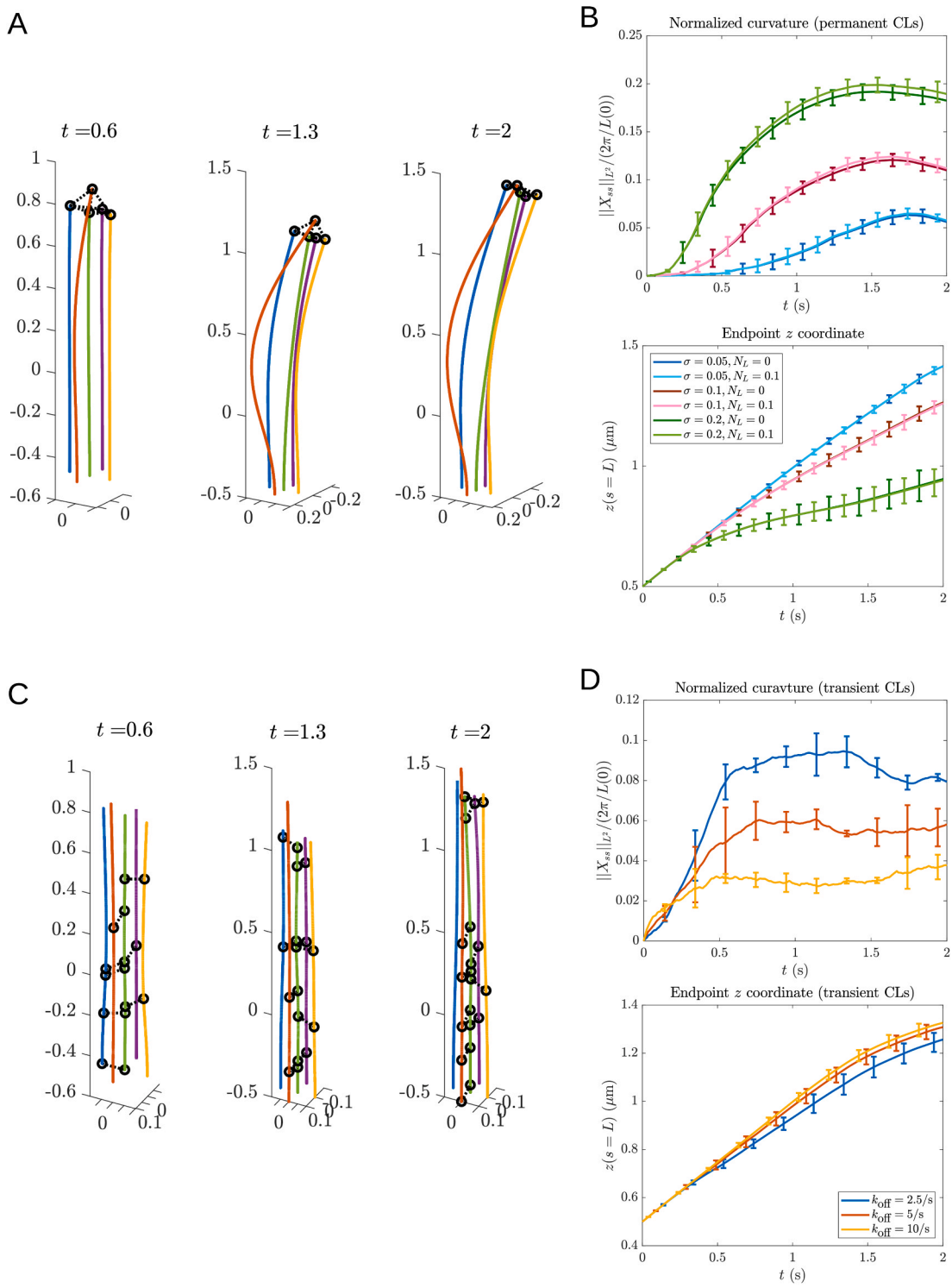

Fig. 2. Lower variance in polymerization rates and dynamic crosslinking alleviate buckling. (A) Simulation of the five-filament bundle with unequal polymerization rates (drawn at $t = 0$ from a normal distribution with mean 0.5 μm/s and standard deviation 0.1 μm/s). Cross links at the tip are permanent in this case, and filaments are color-coded for visualization. (B) Statistics for five-filament filopodial bundle with the tips of the outer filaments permanently crosslinked to the tip of the central filament. The growth rate of each filament is constant in time, but each filament's growth rate is drawn from a normal distribution with mean 0.5 μm/s and varying standard deviation (the values we use are $\sigma = 0.2$, 0.1, and 0.05 μm/s). We plot the average z (in μm) coordinate of the filament endpoints and the average filament curvature (normalized by the curvature of a circle with the same circumference as the filament length) as functions of time (in seconds). We are considering the mean over ten samples, with the error bars showing the standard error of the mean. The lighter colors are when no active torque is applied ($N_L = 0$), while the darker colors show the case when formin at the tip of each growing fiber generates a torque with value $N_L = 0.1$ pN $\cdot$ μm. (C) Simulation of the same bundle as in (A) (with the same growth rates), but with transient cross linkers with off rate $k_{off} = 2.5/s$ (mean residence time 0.4 s). (D) Statistics for five-filament filopodial bundle with transient crosslinkers. We fix $k_{on}/k_{off} = 0.02$, so that the average number of links is roughly constant. Between the simulations, we vary parameter k_{off} (2.5/s – blue curves, 5/s – red curves, and 10/s – yellow curves). We plot the average z (in μm) coordinate of the filament endpoints and the average filament curvature (normalized by the curvature of a circle with the same circumference as the filament length) as functions of time (in seconds). We are considering the mean over ten samples, with the error bars showing the standard error of the mean.

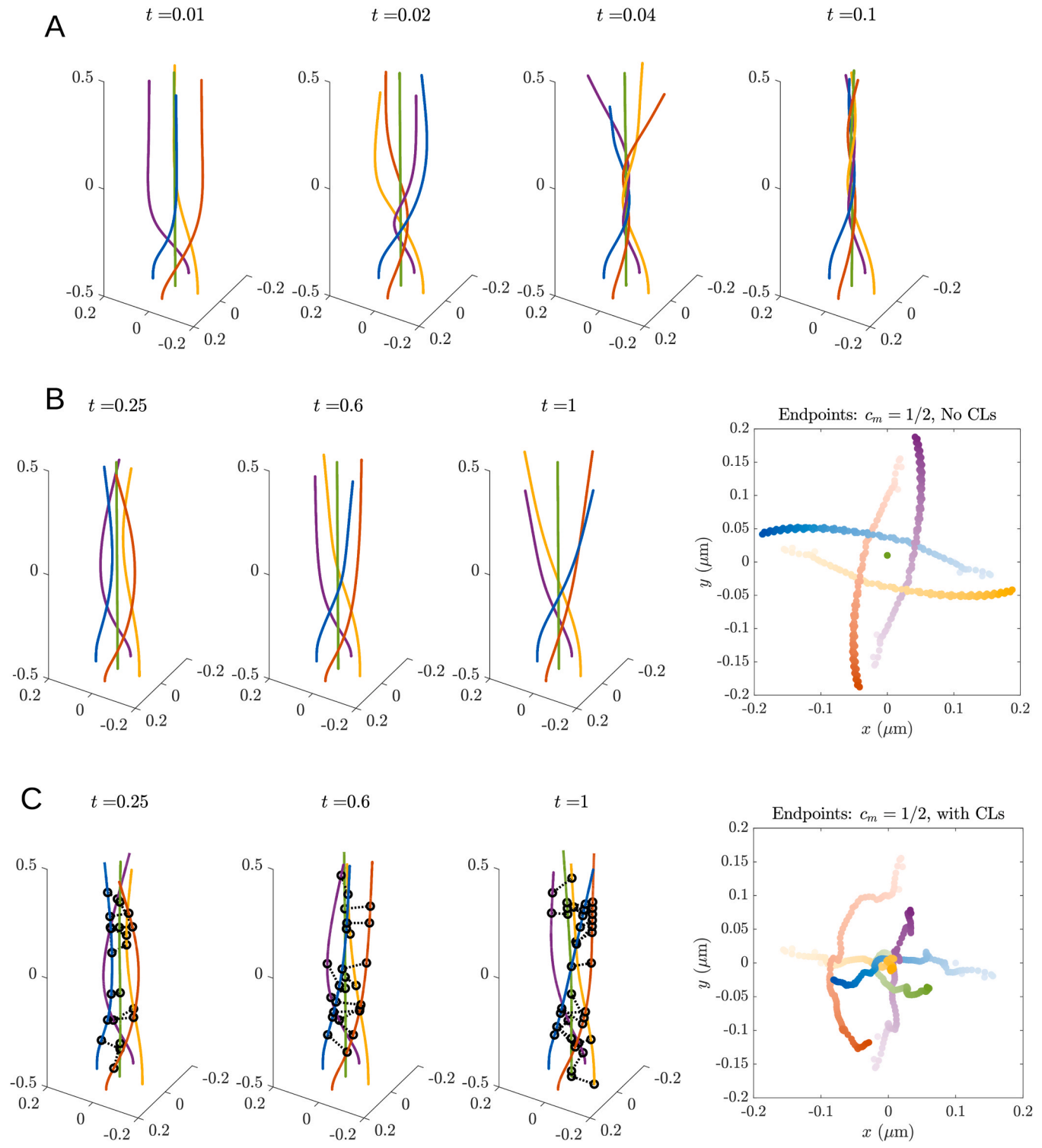

Fig. 3. Motors acting on filopodium edges effectively braid the fibers, but at the cost of loss of compactness. (A) Time sequence of a five-filament "bundle" (no cross links) when the motors act on the edges of the filopodium, and along the whole length of the filaments ($c_m = 1$). Filaments are color-coded for visualization. Time is in seconds, distances are in μm. (B) The same time sequence, but when the motors act only along *half* the length of the fiber ($c_m = 1/2$). The right-most image shows a 2D projection of the fiber endpoints over time. The colors correspond to the fiber colors in the images at left, and darker dots show positions at later time points. (C) Time sequence when motors act along half length of the fiber ($c_m = 1/2$), and transient cross linkers act to keep the bundle compact. The right-most image shows a 2D projection of the fiber endpoints over time. The colors correspond to the fiber colors in the images at left, and darker dots show positions at later time points.

As we already observed in the five-filament case, the twisting of the filaments at the tips makes little difference if there is no motor activity (Fig. 4B). Without motor activity, filaments basically grow straight outward, segregating from time to time into mini-bundles by the crosslinkers, but there is no discernible chirality. When we add motors, but remove twist, we see a braid coming together, but the packing appears fairly loose (Fig. 4C), with filaments growing apart at the top of the bundle, as we already saw in the five-filament case (Section 3.2). By

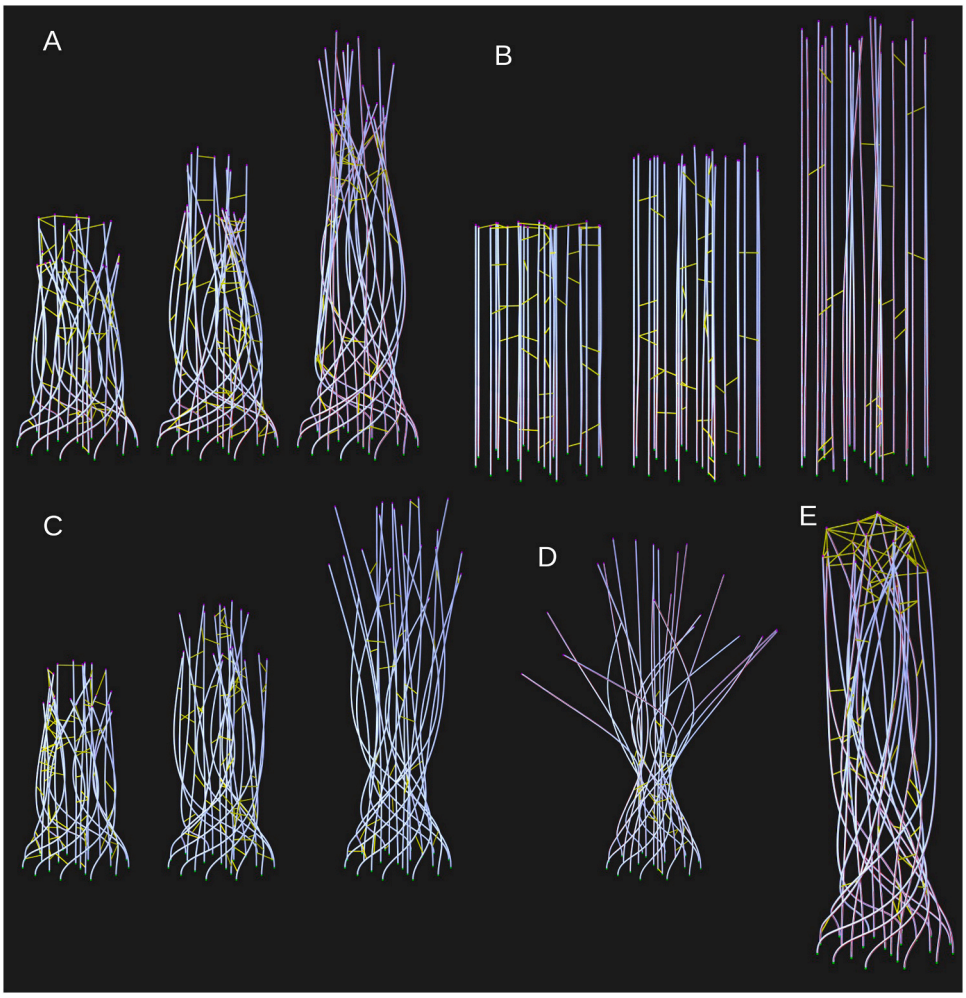

Fig. 4. Snapshots of 22-filament bundles with and without motor and twisting activity, showing that motors and twist synergize to generate a compact bundle. Crosslinks are shown in yellow, filaments in white, and formins in magenta. The green dots show the clamped ends, which represent the branched actin network beneath the filopodium. (A) Time sequence of filopodium growth when there is both formin twisting and motors acting along the half length of the fiber ($c_m = 1/2$). Snapshots are shown at $t = 0.2$, 0.8, and 2 s. See supplementary movie 1 for full sequence. (B) Time sequence of filopodium growth when there is only formin twisting, and no motor activity. Snapshots are shown at $t = 0.2$, 0.8, and 2 s. See supplementary movie 2 for full sequence. (C) Time sequence of filopodium growth when there is only motor activity, and no formin twisting. Snapshots are shown at $t = 0.2$, 0.8, and 2 s. See supplementary movie 3 for full sequence. (D) Snapshot from the end of a simulation ($t = 2$ s) when formins move in the opposite direction (CW, looking from the tip) from the motors (CCW, looking from the tip). See supplementary movie 4 for full sequence. (E) Snapshot from the end of a simulation ($t = 2$ s) when crosslinks at the tip are permanent (a sort of filopodial tip complex; in the simulations, permanent crosslinks connect the plus ends that are the nearest neighbors), while crosslinks below the tip are free to bind and unbind transiently. A less compact bundle with more bending and buckling is observed.

contrast, when we add formin twisting to the motor activity, we see a bundle which is significantly tighter and with filaments that are wound more around the central fiber (Fig. 4A).

3.3.1. *Positive twist at the tip pushes filaments into the center of the filopodium*

To verify that these more compact bundles are not due to random chance, we study the final position (at $t = 2$ s) of the peripheral filament plus ends. In Fig. 5A we plot the endpoints of the outer 12 fibers in the filopodium across ten simulations, projected onto the (x, y) plane. In addition to plotting simulations with CCW formin twist and no motors (blue circles) and motors and no twist (black diamonds), we plot simulations with motor activity and twisting. The red squares show when the formin torque is applied in the same CCW direction as the motors, while the green triangles show the endpoints when the torque is applied in the *opposite* CW direction (Fig. 4D gives an impression of the end position of sample simulations). The significant change from a compact set of the plus ends' ending positions (when the torque is in the same direction) to a very large outward splaying of the plus ends' ending positions (when the torque is in the opposite direction), shows how formin twist in the same (CCW) direction as motor spin is vital in maintaining a tight filopodium shape. Indeed, the filopodium with motors and twist is actually tighter than without motors.

To quantify this effect, we define filopodium compaction as the mean $R = \sqrt{x^2 + y^2}$ coordinate of the peripheral fiber endpoints. We compute the mean across five simulations (60 total fibers), then repeat across the second set of five to generate error bars. Fig. 5B shows how compaction changes when we vary the motor/formin twist model. The colors and shapes of the symbols correspond to those in Fig. 5A; thus, the mean compaction of filopodia with formin twist and no motors is about 0.3, while the compaction for formin twist and motors is roughly 0.15. There is a small but significant increase in R (decrease in compaction) when we introduce motors without the formin twist, on the order of 10–15%. Fig. 5C shows a kind of phase diagram of compaction (R) as a function of the motor force density $f_{\text{mot}}^{(0)}$ and formin twist N_L. As already noted, R is smallest (compaction best) when the formin torque and motor force have the same sign, and worst when they have opposite signs. The

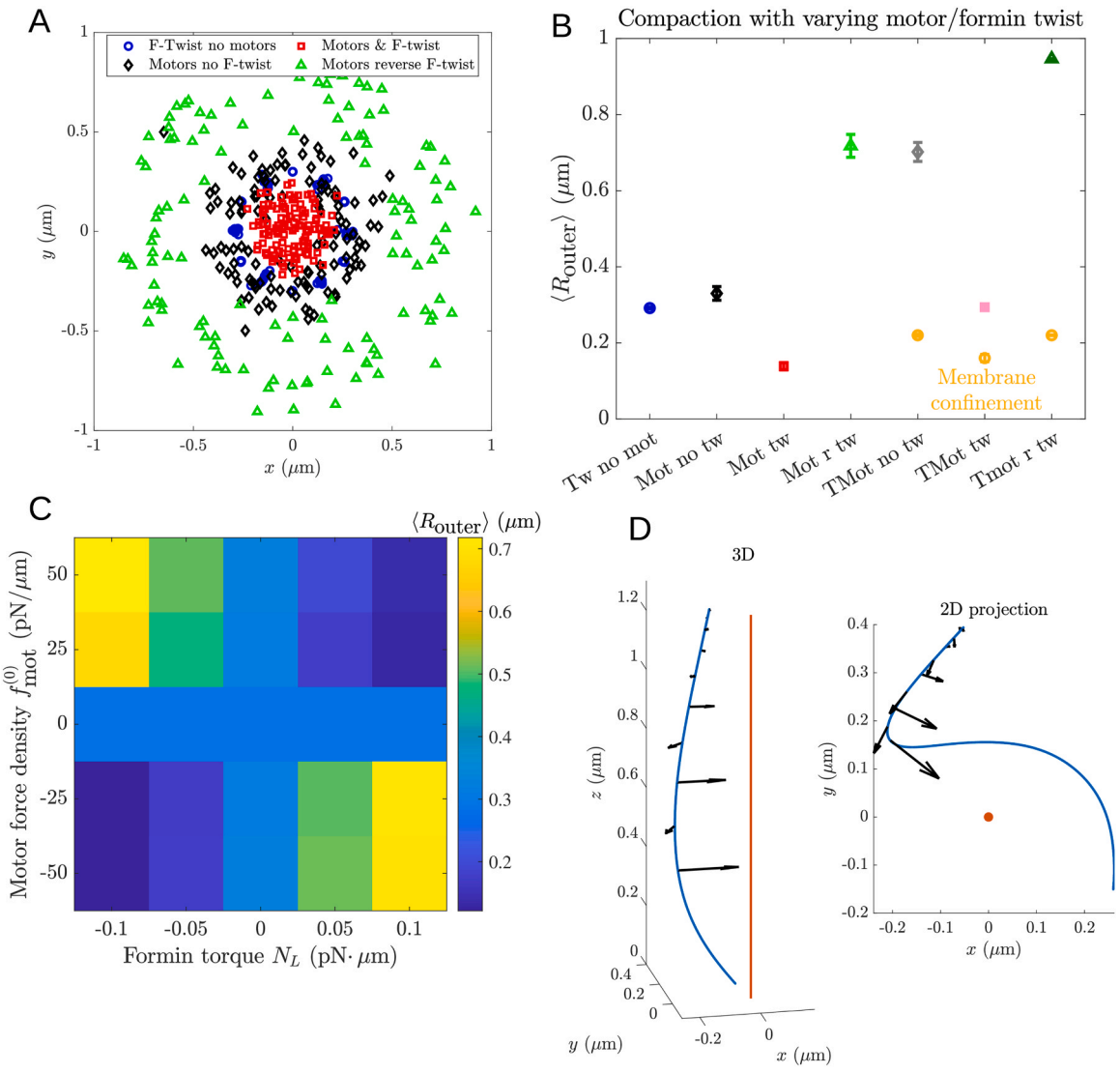

Fig. 5. Compaction is driven by twist forces activated by bending. (A) The positions of the outer 12 filaments' tips at $t = 2$ s, projected onto the (x, y) plane for three simulation conditions. Blue circles correspond to twist without motors, black diamonds correspond to motors without twist, and red squares correspond to motors with twist. The green triangles correspond to what happens when we reverse the direction of formin twisting. Simulations were repeated 10 times for each parameter set. (B) To quantify the data in (A), we define $\langle R_{\text{outer}} \rangle$ as the mean radial coordinate of the endpoints at $t = 2$. Smaller $\langle R_{\text{outer}} \rangle$ then makes for better compaction. We consider simulations with a variety of parameters here. For formins, we use the shorthand "tw" to denote simulations that include CCW formin twist, "no tw" to denote simulations that do not include formin twist, and "r tw" to denote simulations that include CW (reverse) formin twist. For the motors, we use "mot" to denote motors that apply forces, and "TMot" to denote motors with both forces and torques applied to the fibers. For motors with torques, we also plot results that include membrane confinement as yellow circles. See Fig. S9 for more details on this. (C) Phase diagram of $\langle R_{\text{outer}} \rangle$ as a function of formin torque N_L (pN $\cdot$ μm) and motor force density $f^{(0)}_{\text{mot}}$ (pN/μm) (motors only exert force here). Darker blue colors represent better compaction. (D) Shape of an outer filament (in 3D and projection onto the (x, y) plane) in the 22-filament filopodium as computed when the motors apply force to the lower half of the bundle, but without the formin twist. We show the resulting forces on the upper region of the filament (arrows) generated when we apply formin twist and the twist angle assumes its steady state. The red line (circle in the 2D projection) shows the central (z) axis of the filopodium.

compaction appears to depend much more strongly on formin torque than motor force, which indicates that the twist density of the fibers has a strong effect on compaction.

To understand this effect, we isolate a filament *from a simulation without twist* and compute the twist force:

$$\boldsymbol{f}^{(\gamma)} = \gamma \partial_s \left(\psi \left(\partial_s \mathbb{X} \times \partial_s^2 \mathbb{X} \right) \right) = \gamma \psi \left(\partial_s \mathbb{X} \times \partial_s^3 \mathbb{X} \right) \tag{2}$$

when the twist angle $\psi = N_L/\gamma$ is in its constant steady state (this is how the second equality follows from the first). Here γ is the torsional rigidity of actin, N_L is the formin torque, and $\mathbb{X}$ is the 3D curve of the filament centerline (see the SM for details). The fiber and the twist force density on its top half (where motors do not act) are shown in Fig. 5D. There, we see that the twist force is largely directed towards the center of the filopodium, as is qualitatively clear from the large bundle simulations. Equation (2) also shows why the twist force is only significant when motors bend the fibers: the force density is only nonzero when $\partial_s^3 \mathbb{X}$ is nonzero. Thus, when fibers are straight, as is the case when motors are absent, the twist force is zero, and there is no way for the twist to feed back onto the fiber shape. It is necessary for the motors to first bend the fibers, and then formin twist can affect the shape. Thus, the motors and formins synergize to make the bundle more compact.

Given that we need strong bending of the fibers by the motors to activate the twist force, we might expect a decrease in compaction when we decrease the domain of motor activity. In Fig. S4, we show a sample filopodium at $t = 2$ and the corresponding statistics for curvature when

we drop the motor range to the lower 1/4 of the filaments (from 1/2) and outer 1/8 of the circle (from 1/4). We see less bending, and the outward splaying that is characteristic of simulations with insufficient twist force to give contractility (the compaction statistic is $\langle R_{\text{outer}}\rangle = 0.44 \pm 0.02$). Because this effect comes from the fiber curvature and not the formin twist, it is not rescued when we increase the formin twist by a factor of two ($\langle R_{\text{outer}}\rangle = 0.43 \pm 0.02$ for $N_L = 0.2$ pN $\cdot\ \mu$m and the smaller motor range). However, the right panel of Fig. S4 shows that formin twist still draws the filaments inwards, as reversing the direction gives much less compaction ($\langle R_{\text{outer}}\rangle = 0.67 \pm 0.01$ for $N_L = -0.1$ pN $\cdot\ \mu$m and the smaller motor range). Thus the synergy of formin and motors is still there, but its effect is less pronounced when motors do not act as strongly to bend the filaments.

3.3.2. Exploring more realistic helical motor force

In our simplified model of motor forcing, we assume that motors only exert forces in the (x, y) plane perpendicular to the filopodial axis, regardless of the orientation of the filament tangent vector. In reality, motors generate power strokes along the helical path on filaments, and exert forces both tangential to the centerline (towards the base of the fiber) and perpendicular to the centerline. The particular balance of this force is dictated by the type of motor considered; some motors move exactly along the helical pitch of the filament (Norstrom et al., 2010), thus exerting the corresponding ratio of force in the normal to tangential direction. Most motors, however, do not exactly follow this trajectory, sometimes skipping monomers along the filament (Ali et al., 2002b; Tominaga et al., 2003), and consequently have a force which is dominated by the tangential direction. For the case of a motor walking along the helical path, the schematic diagram in Fig. S5 shows how motor activity changes when the filament orientation changes. The left panel shows the filament in blue with its helical path in yellow. The force that the motor exerts is then in the opposite direction of the helical path, and contains a direction both normal and parallel to the filament. In the case when the filament is vertical (tangent vector in the $+z$ direction), then the dominant force is normal to the filament, as we have already implemented. But if the filament orientation changes to become more horizontal (x direction), the dominant motor force becomes more and more downward ($-z$ direction), and there is a corresponding force in the $-x$ direction due to the helicity of the filament. Thus, it is possible that more realistic treatment of the forces might prevent us from accessing the regime where filaments are sufficiently bent to activate twist elasticity.

To explore this, we generalize our procedure for computing motor forces as follows: given a point $\boldsymbol{X}(s)$ on the filament, we compute its cylindrical coordinates (R, θ, z). We then use these coordinates to construct a vector from the filopodial sheath to the filament which points in the inward normal direction, $\boldsymbol{r} = -(\cos\theta, \sin\theta, 0)$. We make this vector orthogonal to the filament by projecting off the tangent vector $\boldsymbol{\tau}(s)$ direction. The motor force then has two components: f_0 in the $\widehat{\boldsymbol{r}}^{\perp}(s) = \widehat{\boldsymbol{r}}(s) \times \boldsymbol{\tau}(s)$ direction, and $3f_0/8$ in the $-\boldsymbol{\tau}(s)$ direction, where the ratio is chosen to match the helical pitch of actin filaments (Dominguez and Holmes, 2011).

We perform a set of simulations with this motor forcing, finding that the integrity of the bundle is completely destroyed (left panel of Fig. S5), because the large downward ($-z$) and compressive ($-\boldsymbol{\tau}$) forces on outer filaments coil them and press to the filopodial base. Actual filopodial architectures do *not* resemble this configuration, and we conclude that the retrograde flow must alleviate these forces. The molecular biophysical basis for this assumption is that the motors are characterized by force-velocity relations, and if a filament moves in the direction of the motor power strokes, then the motor force decreases. We consider two possibilities for the retrograde flow: in the first case, there is a local flow in the $-\boldsymbol{\tau}$ direction on each filament which eliminates the *compressive* force from the motors in the $-\boldsymbol{\tau}$ direction, but not the downward force from the $\widehat{\boldsymbol{r}}^{\perp}(s)$ direction. As shown in the middle frame of Fig. S5, implementing only the force in the $\widehat{\boldsymbol{r}}^{\perp}(s)$ direction (which still changes with the filament orientation) leads to a more ordered bundle, but still causes a significant net downward motion on the outer filaments, such that they coil around the base in the (x, y) plane. If we instead implement a global retrograde flow which cancels the *downward* forces (any forces in the $-z$ direction), we can still retain the compressive forces and get reasonable dynamics, shown in the right panel of Fig. S5. Simply put, these dynamics contain the same assumptions as our original simulations (retrograde flow cancels the force in the $-z$ direction), but have a motor forcing in the planar directions which evolves with the motor geometry.

To test whether the changing motor geometry significantly impacts our results, we consider simulations with the motor forcing $\boldsymbol{f}^{(\text{mot})} = f_0^{(\text{mot})}(\boldsymbol{I} - \widehat{z}\widehat{z})(\widehat{\boldsymbol{r}}^{\perp} - 3/8\boldsymbol{\tau})$, so that the motor force depends on the local filament orientation, but its downward component is attenuated by the retrograde flow. In Fig. S6, we compare the number of rotations around the central filament and the amount of compaction for three different values of the formin twist, finding that the values we obtain are roughly unchanged when we consider this more realistic forcing. Thus, our simplified force model does not impact the overall conclusions, provided that we assume a retrograde flow cancels potentially large downward forces on the filopodium.

3.3.3. Motor torque and deformable membrane

So far, we have neglected the possibility that motors also apply torque to the filament centerlines. Indeed, if the motor action occurs on the fiber boundary rather than the centerline, then motors should exert both a force density and torque density on the fibers. In the SM, Fig. 5B and Figs. S7–S9, we report our results when we repeat the simulations of Section 3.3.1 with the simple change that motor action (along the bottom half of the peripheral fibers) also introduces torque in the same direction as the motor forces (CCW). The result is that the motor torque undoes some of the torque applied by formins, which decreases the amount of compaction for a fixed set of parameters. This makes formin torque all the more vital to prevent extreme outward movement of the filament tips; Fig. 5B shows the compacting effect of formin twist is more drastic in the case when we include motor torque (compare pink square to gray diamond). With formin and motor torque, the radial coordinates of the peripheral filaments are the same at the beginning and end of the simulation (0.3 μm).

Another way to prevent outward motion of the filaments is to confine the filopodial bundle by introducing a deformable membrane. We model this by introducing a normal force which tends to keep the fibers inside of a ring of certain radius. In the SM, Fig. 5B and Fig. S9, we illustrate this effect, the result of which is to introduce a ceiling on the final value of the compaction radius. Fig. 5B (yellow circles) shows that including formin torque still provides additional compaction.

3.4. Role of transient cross linking and variable growth rates

To conclude our study, we return to our original assertion that more permanent crosslinking and more variable growth rates should impact the buckling in the bundle. To study this, we perform the simulations with motor and formin torque, as in Section 3.3.3, but with more variable polymerization rate or slower crosslink dynamics (see details in SM). In Fig. S11, we demonstrate quantitatively that increasing the variance in the fiber growth rate or making the crosslink dynamics slower (see details in SM) leads to increased buckling. We find that, while the trajectories of the outer filaments in the bundle are dominated by the motors and therefore do not change substantially, the inner filaments tend to buckle more under variable growth rates and more permanent crosslinks, in accordance with our observations in Section 3.1. We also find a correlation between buckling and compaction, as compaction tends to correlate with filaments that are *not* buckled, which happens when they all grow at a constant length and have rapidly

exchanging crosslinks.

It is indeed a strange result that transient (rather than permanent) crosslinking aids compaction, since permanent crosslinks should act as an attractive potential between fibers. We found that the relationship is non-monotonic: if there are no crosslinks, the bundles are less compact than both the base parameter value and the value for longer crosslink residence times. Thus when crosslink residence times are too long, the attractive potential can give strange constraints on the trajectories, which leads to buckling and poor compaction. At the opposite end of the spectrum, filaments without crosslinks do have a small outward displacement. There is an optimal crosslink turnover rate when the links are on long enough to promote attraction, but not too long to lead to buckling.

As an example of how permanent crosslinks can constrain fiber trajectories, we consider a simulation where the crosslinks at the fiber plus ends are permanent, mimicking the filopodial tip complex, while crosslinks connecting the filaments' sides can form and break dynamically. Fig. 4E shows the resulting filopodium (without twisting motors, to be consistent with the other plots in Fig. 4). Comparing to Fig. 4A, we observe significantly more bending of the interior fibers and a much wider bundle, as the filopodial tip complex provides an additional constraint preventing the filaments from being drawn into the middle. In addition, the filaments appear more buckled because of the variance in the polymerization rate, and there is a direction of bending to the filopodium, similar to what we saw earlier in five-filament bundles with permanent crosslinks. These qualitative conclusions are confirmed qualitatively in Fig. S12, where we plot the mean curvature and z coordinate in simulations with motor twist and the permanent cross links at the fiber endpoints. Compared to the left panels in Fig. S11, which show the base parameters, the simulations with permanent CLs at the end display more curvature of the inner circles of filaments.

4. Discussion

We found that the spinning action by helical motors effectively "braids" the actin bundle, compacting it, generating buckling, and enhancing the crosslinking. Stochastic fluctuations of actin polymerization rates also contributed to filament buckling and bending of the bundle. Faster turnover of transient crosslinks attenuated the buckling but could enhance coiling and compaction of the bundle. Interestingly, formin-generated twisting alone was much less effective than myosin-generated spinning in inducing filopodial braiding and compaction, but formin action helped the motors to compact the bundle once braided. Indeed, we found that in the absence of confining membrane forces, co-rotating formin action is *necessary* to maintain a compact bundle.

Our model prediction that myosin action, as opposed to formin activity, is the key for coiling the filopodium, is in agreement with the observation that the molecular activities of myosin V and X are involved in rotation of filopodia whereas the formin mDia1 does not play a role in the observed rotations (Leijnse et al., 2022). We note though that formins may not rotate or twist filaments (Kovar and Pollard, 2004), which could be an alternative explanation of why perturbations of formin reported in (Leijnse et al., 2022) did not inhibit the chiral filopodial structure. Another observation from our simulations – that buckling of several filaments that grow faster than others can create an actin loop and respective bulge at the filopodial tip – could be relevant to similar experimentally-observed structures (Li et al., 2023). The mechanisms we discussed here could also be relevant to processes that trigger chiral tilting of actomyosin fibers in adherent cells (Tee et al., 2015). Some of these mechanisms are very similar to microtubule/kinesin interactions generating chirality of the mitotic spindle (Novak et al., 2018).

One of the model predictions – that faster crosslink turnover enhances coiling and compaction in the filopodium – is nontrivial and probably could be tested in future experiments. The two main crosslinkers in filopodia are α-actinin and fascin (Courson and Rock, 2010). Here we tested crosslinking with very rapid kinetics on the scale of several cycles of binding/unbinding per second, which is characteristic of α-actinin (Wachsstock et al., 1994). Another principal crosslinker in filopodia, fascin, has much slower kinetics with the turnover cycle on the scale of 10 s (Aratyn et al., 2007), which implies that the bundle chirality could be sensitive to the concentration ratio between ubiquitous crosslinkers, and could explain why bundle chirality is not universally observed. A simple prediction of the longer residence time is that we should observe more buckling in filopodia crosslinked by fascin compared to α-actinin. Another interesting prediction for the future is that the filopodial bundle chirality is the same as that of the helical myosin motors: if the motors spin filaments CW (CCW), then the bundle will coil CW (CCW), respectively. The predicted effect of formin depends on the relative helicity of the motors and formin: if formin-generated torque rotates filaments in the same direction as the motors, then the bundle will be tighter; if the formin torque is opposite to the motor spinning action, then the bundle will be more disheveled. The most straightforward way to test the model predictions would be (difficult) in vitro experiments, for example growing actin bundles in micro-wells (Colin et al., 2023) with crosslinkers in the solute and with myosins and formins coating different parts of the micro-well surface.

What could be the possible roles of the spinning and twisting actions of the myosins and formins, respectively, and of the resulting coiling and buckling of the filopodial bundles? One very suggestive role, based on the simulations, is the compaction of the bundle, which likely means greater mechanical stability. Mechanical stability of the bundle is, in fact, affected by coiling even without compaction (Daniels and Turner, 2013). Another possibility is that the spinning action could result in rotation of the filopodia around axes not coinciding with bundle axes, as was observed in (Tamada et al., 2010), which could allow filopodia scanning over a greater area around the cell edge. Some filopodia fold back into the cell leading edge and contribute to construction of contractile bundles in the lamella (Nemethova et al., 2008), and in that way pre-established filopodial chirality could trigger larger scale chirality of the cell cortex by interaction with other cytoskeletal structures of the cortex. Coiling and buckling in the filopodial bundle can induce pulling and traction at the tip (Leijnse et al., 2015b). The mechanism of chirality emergence that we explored is but one possibility, and there is likely a diverse inventory of chirality propagation mechanisms, even for just actin bundles. An unknown mechanism, not relying on either myosins or formins, is responsible for a chiral rotation of *Listeria* propelled by a polarized actin tail (Robbins and Theriot, 2003). Turning of long filopodia to the left (Tamada et al., 2010; Li et al., 2023) is not explained by the mechanisms that we considered. General thermodynamic arguments demonstrated that when chiral filaments are bundled, a macroscopic twist is generated in the bundle (Grason and Bruinsma, 2007). It was shown theoretically that crosslink binding to actin filaments along helical patches on the filaments generates intrinsic torques, which wind the bundle superhelically about its central axis (Heussinger and Grason, 2011; Grason, 2015). Recently, a detailed simulation with monomer-scale resolution confirmed that torsional compliance in a finite-width filament can induce chirality in the structure of a crosslinked bundle (Floyd et al., 2022). It was experimentally observed that small rigid actin-binding proteins change the twist of filaments in a concentration-dependent manner, resulting in small, well defined bundle thickness up to 20 filaments (Claessens et al., 2008), which, accidentally or not, is on the order of the filament number in filopodium. Finally, actin bundling by counterions is also predicted to generate chirality (Mohammadinejad et al., 2012).

Adding factors that we ignored in the model will predict even more nontrivial chiral behaviors. These factors include, but are not limited to: 1) mechanical coupling of twisting and bending, even for a single filament (De La Cruz et al., 2010); 2) complex structure and mechanics of the filopodial protein tip complex (Cheng and Mullins, 2020); 3) formin sensing both force and torque during actin filament polymerization (Yu et al., 2017); 4) multi-stack structure of the fast-growing filopodial

bundle (Medalia et al., 2007; Breitsprecher et al., 2011). Inclusion of these factors into the model and scaling up the simulations will allow us to address the open question about how chirality propagates to the cellular (Tee et al., 2015; Zaatri et al., 2021) and multicellular scales (Yashunsky et al., 2022; Tee et al., 2023).

CRediT authorship contribution statement

Mogilner Alex: Writing – review & editing, Writing – original draft, Supervision, Resources, Project administration, Funding acquisition, Formal analysis, Conceptualization. **Maxian Ondrej:** Writing – review & editing, Writing – original draft, Visualization, Software, Methodology, Investigation, Funding acquisition, Formal analysis, Data curation.

Declaration of Competing Interest

The authors have no competing interests to declare.

Data Availability

Code for the simulations is available at the github repository https://github.com/stochasticHydroTools/SlenderBody/tree/master/Matlab/MainPrograms/Filopodium.

Acknowledgements

This work was supported by the National Science Foundation through Research Training Group in Modeling and Simulation under award RTG/DMS-1646339 and through the Division of Mathematical Sciences awards DMS-2052515 and DMS-1953430. Ondrej Maxian was supported by the NSF via GRFP/DGE-1342536, and by the Chicago-Yen fellowship at the University of Chicago. We thank A. Bershadsky for help with literature and fruitful discussions. Code for simulations can be found at https://github.com/stochasticHydroTools/SlenderBody/tree/master/Matlab/MainPrograms/Filopodium.

Appendix A. Supporting information

Supplementary data and movies associated with this article can be found in the online version at doi:10.1016/j.ejcb.2023.151383.

References

Ali, M.Y., Uemura, S., Adachi, K., Itoh, H., Kinosita Jr, K., Ishiwata, S., 2002a. Myosin V is a left-handed spiral motor on the right-handed actin helix. Nat. Struct. Biol. 9 (6), 464–467.
Ali, M.Y., Uemura, S., Adachi, K., Itoh, H., Kinosita Jr, K., Ishiwata, S., 2002b. Myosin v is a left-handed spiral motor on the right-handed actin helix. Nat. Struct. Biol. 9 (6), 464–467.
Alieva, N.O., Efremov, A.K., Hu, S., Oh, D., Chen, Z., Natarajan, M., Ong, H.T., Jégou, A., Romet-Lemonne, G., Groves, J.T., Sheetz, M.P., Yan, J., Bershadsky, A.D., 2019. Myosin IIA and formin dependent mechanosensitivity of filopodia adhesion. Nat. Commun. 10 (1), 3593.
Aratyn, Y.S., Schaus, T.E., Taylor, E.W., Borisy, G.G., 2007. Intrinsic dynamic behavior of fascin in filopodia. Mol. Biol. Cell 18 (10), 3928–3940.
Arjonen, A., Kaukonen, R., Ivaska, J., 2011. Filopodia and adhesion in cancer cell motility. Cell Adh. Migr. 5 (5), 421–430.
Beausang, J.F., Schroeder 3rd, H.W., Nelson, P.C., Goldman, Y.E., 2008. Twirling of actin by myosins II and V observed via polarized TIRF in a modified gliding assay. Biophys. J. 95 (12), 5820–5831.
Berro, J., Michelot, A., Blanchoin, L., Kovar, D.R., Martiel, J.-L., 2007. Attachment conditions control actin filament buckling and the production of forces. Biophys. J. 92 (7), 2546–2558.
Bibeau, J.P., Pandit, N.G., Gray, S., Nejad, N.S., Sindelar, C.V., Cao, W., De La Cruz, E.M., 2023. Twist response of actin filaments. Proc. Natl. Acad. Sci. 120 (4), e2208536120.
Breitsprecher, D., Koestler, S.A., Chizhov, I., Nemethova, M., Mueller, J., Goode, B.L., Small, J.V., Rottner, K., Faix, J., 2011. Cofilin cooperates with fascin to disassemble filopodial actin filaments. J. Cell Sci. 124 (Pt 19), 3305–3318.
Cheney, R.E., O'Shea, M.K., Heuser, J.E., Coelho, M.V., Wolenski, J.S., Espreafico, E.M., Forscher, P., Larson, R.E., Mooseker, M.S., 1993. Brain myosin-v is a two-headed unconventional myosin with motor activity. Cell 75 (1), 13–23.
Cheng, K.W., Mullins, R.D., 2020. Initiation and disassembly of filopodia tip complexes containing VASP and lamellipodin. Mol. Biol. Cell 31 (18), 2021–2034.
Chesarone, M.A., DuPage, A.G., Goode, B.L., 2010. Unleashing formins to remodel the actin and microtubule cytoskeletons. Nat. Rev. Mol. Cell Biol. 11 (1), 62–74.
Claessens, M.M.A.E., Semmrich, C., Ramos, L., Bausch, A.R., 2008. Helical twist controls the thickness of f-actin bundles. Proc. Natl. Acad. Sci. 105 (26), 8819–8822.
Colin, A., Kotila, T., Guérin, C., Orhant-Prioux, M., Vianay, B., Mogilner, A., Lappalainen, P., Théry, M., Blanchoin, L., 2023. Recycling of the actin monomer pool limits the lifetime of network turnover. EMBO J. 42 (9), e112717.
Courson, D.S., Rock, R.S., 2010. Actin cross-link assembly and disassembly mechanics for alpha-actinin and fascin. J. Biol. Chem. 285 (34), 26350–26357.
Daniels, D.R., Turner, M.S., 2013. Islands of conformational stability for filopodia. PLoS One 8 (3), e59010.
Davenport, R.W., Dou, P., Rehder, V., Kater, S.B., 1993. A sensory role for neuronal growth cone filopodia. Nature 361 (6414), 721–724.
De La Cruz, E.M., Roland, J., McCullough, B.R., Blanchoin, L., Martiel, J.-L., 2010. Origin of twist-bend coupling in actin filaments. Biophys. J. 99 (6), 1852–1860.
Dominguez, R., Holmes, K.C., 2011. Actin structure and function. Annu. Rev. Biophys. 40, 169–186.
Evans, L.L., Hammer, J., Bridgman, P.C., 1997. Subcellular localization of myosin V in nerve growth cones and outgrowth from dilute-lethal neurons. J. Cell Sci. 110 (Pt 4), 439–449.
Fierro-González, J.C., White, M.D., Silva, J.C., Plachta, N., 2013. Cadherin-dependent filopodia control preimplantation embryo compaction. Nat. Cell Biol. 15 (12), 1424–1433.
Fletcher, D.A., Mullins, R.D., 2010. Cell mechanics and the cytoskeleton. Nature 463 (7280), 485–492.
Floyd, C., Ni, H., Gunaratne, R.S., Erban, R., Papoian, G.A., 2022. On stretching, bending, shearing, and twisting of actin filaments i: variational models. J. Chem. Theory Comput. 18 (8), 4865–4878.
Forscher, P., Smith, S.J., 1988. Actions of cytochalasins on the organization of actin filaments and microtubules in a neuronal growth cone. J. Cell Biol. 107 (4), 1505–1516.
Grason, G.M., 2015. Colloquium: geometry and optimal packing of twisted columns and filaments. Rev. Mod. Phys. 87 (2), 401.
Grason, G.M., Bruinsma, R.F., 2007. Chirality and equilibrium biopolymer bundles. Phys. Rev. Lett. 99 (9), 098101.
Heussinger, C., Grason, G.M., 2011. Theory of crosslinked bundles of helical filaments: intrinsic torques in self-limiting biopolymer assemblies. J. Chem. Phys. 135 (3), 035104.
Hu, W., Wehrle-Haller, B., Vogel, V., 2014. Maturation of filopodia shaft adhesions is upregulated by local cycles of lamellipodia advancements and retractions. PLoS One 9 (9), e107097.
Inaki, M., Liu, J., Matsuno, K., 2016. Cell chirality: its origin and roles in left-right asymmetric development. Philos. Trans. R. Soc. Lond. B Biol. Sci. 371 (1710).
Jacquemet, G., Hamidi, H., Ivaska, J., 2015. Filopodia in cell adhesion, 3D migration and cancer cell invasion. Curr. Opin. Cell Biol. 36, 23–31.
Jegou, A., Romet-Lemonne, G., 2020. The many implications of actin filament helicity. Semin Cell Dev. Biol. 102, 65–72.
Kovar, D.R., Pollard, T.D., 2004. Insertional assembly of actin filament barbed ends in association with formins produces piconewton forces. Proc. Natl. Acad. Sci. 101 (41), 14725–14730.
Lan, Y., Papoian, G.A., 2008. The stochastic dynamics of filopodial growth. Biophys. J. 94 (10), 3839–3852.
Lebreton, G., Géminard, C., Lapraz, F., Pyrpassopoulos, S., Cerezo, D., Spéder, P., Ostap, E.M., Noselli, S., 2018. Molecular to organismal chirality is induced by the conserved myosin 1D. Science 362 (6417), 949–952.
N. Leijnse, L.B. Oddershede, and P.M. Bendix.Helical buckling of actin inside filopodia generates traction.Proceedings of the National Academy of Sciences, 112(1): 136–141, 2015b.
Leijnse, N., Oddershede, L.B., Bendix, P.M., 2015a. An updated look at actin dynamics in filopodia. Cytoskelet. (Hoboken) 72 (2), 71–79.
Leijnse, N., Barooji, Y.F., Arastoo, M.R., Sønder, S.L., Verhagen, B., Wullkopf, L., Erler, J. T., Semsey, S., Nylandsted, J., Oddershede, L.B., Doostmohammadi, A., Bendix, P.M., 2022. Filopodia rotate and coil by actively generating twist in their actin shaft. Nat. Commun. 13 (1), 1636.
Li, W., Chung, W.-L., Kozlov, M.M., Medalia, O., Geiger, B., Bershadsky, A.D., 2023. Chiral growth of adherent filopodia. Biophys. J. 122 (18), 3704–3721.
Li, X., Chen, B., 2022. How torque on formins is relaxed strongly affects cellular swirling. Biophys. J. 121 (15), 2952–2961.
Linkner, J., Witte, G., Zhao, H., Junemann, A., Nordholz, B., Runge-Wollmann, P., Lappalainen, P., Faix, J., 2014. The inverse BAR domain protein IBARa drives membrane remodeling to control osmoregulation, phagocytosis and cytokinesis. J. Cell Sci. 127 (Pt 6), 1279–1292.
Mallavarapu, A., Mitchison, T., 1999. Regulated actin cytoskeleton assembly at filopodium tips controls their extension and retraction. J. Cell Biol. 146 (5), 1097–1106.
Martiel, J.-L., Michelot, A., Boujemaa-Paterski, R., Blanchoin, L., Berro, J., 2020. Force production by a bundle of growing actin filaments is limited by its mechanical properties. Biophys. J. 118 (1), 182–192.
Mattila, P.K., Lappalainen, P., 2008. Filopodia: molecular architecture and cellular functions. Nat. Rev. Mol. Cell Biol. 9 (6), 446–454.
Maxian, O., Sprinkle, B., Peskin, C.S., Donev, A., 2022. Hydrodynamics of a twisting, bending, inextensible fiber in stokes flow. Phys. Rev. Fluids 7 (7), 074101.
Medalia, O., Beck, M., Ecke, M., Weber, I., Neujahr, R., Baumeister, W., Gerisch, G., 2007. Organization of actin networks in intact filopodia. Curr. Biol. 17 (1), 79–84.
Medeiros, N.A., Burnette, D.T., Forscher, P., 2006. Myosin II functions in actin-bundle turnover in neuronal growth cones. Nat. Cell Biol. 8 (3), 215–226.

Mellor, H., 2010. The role of formins in filopodia formation. Biochim. Biophys. Acta 1803 (2), 191–200.
Mizuno, H., Higashida, C., Yuan, Y., Ishizaki, T., Narumiya, S., Watanabe, N., 2011. Rotational movement of the formin mdia1 along the double helical strand of an actin filament. Science 331 (6013), 80–83.
Mohammadinejad, S., Golestanian, R., Fazli, H., 2012. Chiral structure of f-actin bundle formed by multivalent counterions. Soft Matter 8, 3649–3656.
Naganathan, S.R., Middelkoop, T.C., Fürthauer, S., Grill, S.W., 2016. Actomyosin-driven left-right asymmetry: from molecular torques to chiral self organization. Curr. Opin. Cell Biol. 38, 24–30.
Nemethova, M., Auinger, S., Small, J.V., 2008. Building the actin cytoskeleton: filopodia contribute to the construction of contractile bundles in the lamella. J. Cell Biol. 180 (6), 1233–1244.
Nishizaka, T., Yagi, T., Tanaka, Y., Ishiwata, S., 1993. Right-handed rotation of an actin filament in an in vitro motile system. Nature 361 (6409), 269–271.
Norstrom, M.F., Smithback, P.A., Rock, R.S., 2010. Unconventional processive mechanics of non-muscle myosin iib. J. Biol. Chem. 285 (34), 26326–26334.
Novak, M., Polak, B., Simunić, J., Boban, Z., Kuzmić, B., Thomae, A.W., Tolić, I.M., Pavin, N., 2018. The mitotic spindle is chiral due to torques within microtubule bundles. Nat. Commun. 9 (1), 3571.
Powers, T.R., 2010. Dynamics of filaments and membranes in a viscous fluid. Rev. Mod. Phys. 82 (2), 1607F–1615.
Pronk, S., Geissler, P.L., Fletcher, D.A., 2008. Limits of filopodium stability. Phys. Rev. Lett. 100 (25), 258102.
Robbins, J.R., Theriot, J.A., 2003. Listeria monocytogenes rotates around its long axis during actin-based motility. Curr. Biol. 13 (19), R754–R756.
Sheetz, M.P., Wayne, D.B., Pearlman, A.L., 1992. Extension of filopodia by motor-dependent actin assembly. Cell Motil. Cytoskelet. 22 (3), 160–169.
Shemesh, T., Otomo, T., Rosen, M.K., Bershadsky, A.D., Kozlov, M.M., 2005. A novel mechanism of actin filament processive capping by formin: solution of the rotation paradox. J. Cell Biol. 170 (6), 889–893.
Stump, D.M., 2000. Toroidal supercoiling of writhed rods. Proc. Math. Phys. Eng. Sci. 456 (2000), 1979–1995.
Sun, Y., Sato, O., Ruhnow, F., Arsenault, M.E., Ikebe, M., Goldman, Y.E., 2010. Single-molecule stepping and structural dynamics of myosin X. Nat. Struct. Mol. Biol. 17 (4), 485–491.
Svitkina, T.M., Bulanova, E.A., Chaga, O.Y., Vignjevic, D.M., Kojima, S.-I., Vasiliev, J.M., Borisy, G.G., 2003. Mechanism of filopodia initiation by reorganization of a dendritic network. J. Cell Biol. 160 (3), 409–421.
Tamada, A., Kawase, S., Murakami, F., Kamiguchi, H., 2010. Autonomous right-screw rotation of growth cone filopodia drives neurite turning. J. Cell Biol. 188 (3), 429–441.
Tanaka, Y., Ishijima, A., Ishiwata, S., 1992. Super helix formation of actin filaments in an in vitro motile system. Biochim. Biophys. Acta 1159 (1), 94–98.
Tee, Y.H., Shemesh, T., Thiagarajan, V., Hariadi, R.F., Anderson, K.L., Page, C., Volkmann, N., Hanein, D., Sivaramakrishnan, S., Kozlov, M.M., et al., 2015. Cellular chirality arising from the self-organization of the actin cytoskeleton. Nat. Cell Biol. 17 (4), 445–457.
Tee, Y.H., Goh, W.J., Yong, X., Ong, H.T., Hu, J., Tay, I.Y.Y., Shi, S., Jalal, S., Barnett, S.F. H., Kanchanawong, P., et al., 2023. Actin polymerisation and crosslinking drive left-right asymmetry in single cell and cell collectives. Nat. Commun. 14 (1), 776.
Tominaga, M., Kojima, H., Yokota, E., Orii, H., Nakamori, R., Katayama, E., Anson, M., Shimmen, T., Oiwa, K., 2003. Higher plant myosin xi moves processively on actin with 35 nm steps at high velocity. EMBO J. 22 (6), 1263–1272.
Wachsstock, D.H., Schwarz, W.H., Pollard, T.D., 1994. Cross-linker dynamics determine the mechanical properties of actin gels. Biophys. J. 66 (3), 801–809.
Watanabe, T.M., Tokuo, H., Gonda, K., Higuchi, H., Ikebe, M., 2010. Myosin-X induces filopodia by multiple elongation mechanism. J. Biol. Chem. 285 (25), 19605–19614.
Wood, W., Jacinto, A., Grose, R., Woolner, S., Gale, J., Wilson, C., Martin, P., 2002. Wound healing recapitulates morphogenesis in drosophila embryos. Nat. Cell Biol. 4 (11), 907–912.
Yamada, H., Abe, T., Satoh, A., Okazaki, N., Tago, S., Kobayashi, K., Yoshida, Y., Oda, Y., Watanabe, M., Tomizawa, K., Matsui, H., Takei, K., 2013. Stabilization of actin bundles by a dynamin 1/cortactin ring complex is necessary for growth cone filopodia. J. Neurosci. 33 (10), 4514–4526.
Yashunsky, V., Pearce, D.J.G., Blanch-Mercader, C., Ascione, F., Silberzan, P., Giomi, L., 2022. Chiral edge current in nematic cell monolayers. Phys. Rev. X 12 (4).
Yu, M., Yuan, X., Lu, C., Le, S., Kawamura, R., Efremov, A.K., Zhao, Z., Kozlov, M.M., Sheetz, M., Bershadsky, A., Yan, J., 2017. mdia1 senses both force and torque during f-actin filament polymerization. Nat. Commun. 8 (1).
Zaatri, A., Perry, J.A., Maddox, A.S., 2021. Septins and a formin have distinct functions in anaphase chiral cortical rotation in the Caenorhabditis elegans zygote. Mol. Biol. Cell 32 (14), 1283–1292.
Zhang, H., Berg, J.S., Li, Z., Wang, Y., LÅng, P., Sousa, A.D., Bhaskar, A., Cheney, R.E., Strömblad, S., 2004. Myosin-X provides a motor-based link between integrins and the cytoskeleton. Nat. Cell Biol. 6 (6), 523–531.
Zhao, H., Pykäläinen, A., Lappalainen, P., 2011. I-BAR domain proteins: linking actin and plasma membrane dynamics. Curr. Opin. Cell Biol. 23 (1), 14–21.